The Impact of Modal Interactions on Receiver Complexity in OAM Fibers

Reza Mirzaei Nejad, Lixian Wang, Jiachuan Lin, Sophie LaRochelle, and Leslie A. Rusch

IEEE/OSA Journal of Lightwave Technology, (Volume 35, Issue 21) (2017)

Doi: 10.1109/JLT.2017.2751248

https://ieeexplore.ieee.org/document/8031323/

The Impact of Modal Interactions on Receiver Complexity in OAM Fibers

Reza Mirzaei Nejad, Lixian Wang, Jiachuan Lin, Sophie LaRochelle, *Senior Member, IEEE, Fellow, OSA*, and Leslie A. Rusch, *Fellow, IEEE, Fellow, OSA*

***Abstract*— We experimentally study the modal interactions in mode division multiplexing (MDM) links supporting orbital angular momentum (OAM) modes of order zero and one. We use time of flight and channel impulse response measurements to characterize our OAM-MDM link and quantify modal impairments. We examine two OAM fibers with different index profiles and differential mode group delays (DMGD) between supported vector modes. Data transmission experiments probe the impact of modal impairments on digital signal processing complexity and achievable bit error rate for OAM-MDM link. We discuss in particular memory depth requirements for equalizers in separate mode detection schemes, and how memory depth varies with DMGD metrics as well as crosstalk level.**

***Index Terms* — Mode Division Multiplexing (MDM), Orbital Angular Momentum (OAM), Ring Core Fiber (RCF).**

I. Introduction

Optical transport networks using single mode fibers (SMF) are reaching the capacity limit predicted by information theory [1]. Mode division multiplexing (MDM) systems have received extensive attention in recent years as a promising technique to overcome the capacity limit [2], [3]. Two different modal bases, linearly polarized (LP) modes and orbital angular momentum (OAM) modes, are studied [4-10].

Consider two receiver solutions for a D mode, 2 polarizations per mode, MDM system: 1) a monolithic receiver with $2\times D$ inputs that are all time synchronized, captured simultaneously and with data processed as one unit, and 2) D standard receivers, with one receiver per mode and no synchronization or integration between them, with data processed independently. Most demonstrated LP-MDM systems use the monolithic receiver with $2D\times 2D$ multiple-input multiple-output (MIMO) equalizers (full-MIMO) [11], [12]. Reduction of receiver complexity is essential for reasonable power consumption and real time processing. The DSP burden can be reduced by using smaller equalizer blocks, such as using D separate equalizers with D standard receivers. The number of equalizers used in separate mode detection scales linearly with the number of modes, whereas in full-MIMO processing, it scales with the square of the number of modes.

Several research groups have worked to reduce the dimensionality of MIMO equalizers. The use of separate equalizer blocks for each mode group instead of full MIMO equalizer was investigated for LP modes in [13],[14]. Six modes, each with two polarizations, in four mode groups were detected via four independent detectors with 2×2 or 4×4 equalizer blocks; The use of two independent, uncoordinated receivers for two modes (LP_{01} and LP_{11e}) in [15], [16] led to low dimension (2×2) MIMO equalizer (covering polarization demultiplexing per mode). A polarization maintaining fiber supporting six spatial channels required no MIMO and used six separate receivers, one per channel [17].

OAM fibers were introduced and designed for separate mode detection with low modal coupling [18], [19]. In OAM-MDM systems, a demonstration with 4 channels using modes of order zero and one used 2×2 MIMO equalizer for polarization demultiplexing per mode [20]. Another OAM demonstration with 12 channels using mode of order ±5,±6,±7 used only optical polarization demultiplexing to recover the data on each mode [21].

Reducing the MIMO dimensionality results in reducing the DSP burden. The complexity of MIMO processing, however, is governed not only by the number of equalizers (i.e., dimensionality), but also by the memory depth (number of taps) per equalizer. Two linear propagation impairments in MDM systems are related to equalizer block complexity: differential mode group delay (DMGD) and channel crosstalk [22], [23]. We examine the relationship between modal interactions and DMGD among different propagating modes and OAM-MDM DSP complexity in separate mode detection schemes.

We focus on systems supporting OAM_0, i.e., fundamental mode, in two polarizations, and $OAM_{\pm 1}$ mode. We examine two OAM fibers experimentally: a ring core fiber (RCF) [24] and an inverse parabolic graded index fiber (IPGIF) [25]. Each supports OAM_0 and $OAM_{\pm 1}$ modes for distances near to one kilometer. HE_{11} and HE_{21} vector modes carry the data channels in these systems; TE_{01} and TM_{01} modes also propagate in OAM-MDM link, but as parasitic modes, i.e., non-data-carrying modes. We will experimentally investigate the impact of modal interactions among data carrying HE_{11} and HE_{21} modes and their interaction with TE_{01}/TM_{01} modes on receiver bit error rate (BER) performance and equalizers required memory depth requirement. The dissimilar refractive index

Submitted for review on 13 Feb, 2017.

Reza Mirzaei Nejad (reza.mirzaei-nejad.1@ulaval.ca), Jiachuan Lin, Sophie LaRochelle, and Leslie A. Rusch (rusch@gel.ulaval.ca) are with the Centre for Optics, Photonics and Lasers (COPL), Dept. of Electrical and Computer Eng., Université Laval, Québec, Canada, QC G1V 0A6.

Lixian Wang was with the Centre for Optics, Photonics and Lasers (COPL), Dept. of Electrical and Computer Eng., Université Laval. He is now a research scientist at CorActive High-Tech Inc., Québec, QC, Canada, G2C 1S9.

profiles in these fibers lead to different DMGD among vector modes of HE_{11}, HE_{21}, TE_{01} and TM_{01}.

In two separate experiments we previously examined time of flight (ToF) for 1.4 km RCF fiber [26] and impulse responses (IR) for both 1.47 km RCF and 1.1 km IPGIF fibers [27]. In [27] we hypothesized the interactions among TE_{01}/TM_{01} and HE_{21} affected equalizer memory length. In this manuscript, we add ToF results for IPGIF and details of the characterization experiments (setup and results). As further validation of our hypothesis, we examine another length (450 m) of RCF fiber. Only by examining all these results together can we quantify the impact of parasitic modes on equalizer block complexity.

In section II, we discuss the modal interactions in OAM-MDM systems. In section III, we characterize each fiber via ToF and IR measurements. Next we transmit data and evaluate receiver performance. In section IV, we report data transmission results. In section V, we discuss the impact of the modal interactions on required OAM-MDM equalizer memory depth by contrasting the two OAM fibers. In section VI, we conclude the paper.

II. Modal Impairments in OAM-MDM systems

We study the impairments in fibers supporting OAM modes of order zero and one. For OAM modes of order one, there are two OAM modes, OAM_{+1} with right circular polarization (OAM_{+1}^{+}) and OAM_{-1} with left circular polarization (OAM_{-1}^{-}):

$$OAM_{\pm 1}^{\pm} = HE_{21}^{even} \pm i\, HE_{21}^{odd} \tag{3}$$

The two other OAM modes of order one, formed by TE_{01} and TM_{01}, are known to be unstable [28]

$$OAM_{\pm 1}^{\mp} = TE_{01} \pm i\, TM_{01} \tag{4}$$

The unequal effective indices of TE_{01} and TM_{01} modes cause them to travel at different speeds, leading to walk-off and instability. Note that OAM mode of order zero, i.e. without any topological charge, denoted by OAM_0^+ and OAM_0^- are fundamental mode, equivalent to HE_{11} mode with right and left circular polarization respectively.

Contrary to LP-MDM systems using LP_{11} modes where all vector modes of HE_{21}, TE_{01} and TM_{01} are used within data channels, in OAM fibers supporting modes of order one, TE_{01} and TM_{01} modes propagate but are not used as OAM data channels. However, they can have some parasitic effects on data carrying channels which will be investigated.

Fig. 1 illustrates propagation modes in a fiber in an OAM system. $OAM_0^{\pm}$ and $OAM_{\pm 1}$ modes are injected into the fiber via a mode multiplexer. These modes should excite primary vector modes HE_{11} and HE_{21}. Due to undesired crosstalk, there

Table I
Measured DMGD between OAM_0 and OAM_1 mode groups per fiber

Fiber	DMGD (ns) ±0.1 ns			
	($DMGD_{01}$) $HE_{11} - HE_{21}$	$HE_{21} - TM_{01}$	$TE_{01} - HE_{21}$	($DMGD_{11}$) ($HE_{21} - TM_{01}$) + ($TE_{01} - HE_{21}$)
1.1 km IPGIF	31.2	0.5	1.2	1.7
1.47 km RCF	23.9	1.2	2.6	3.8

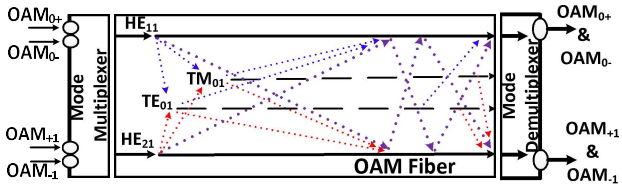

Fig. 1. Channel model for interactions among vector modes propagating in OAM fibers supporting modes of order zero and one.

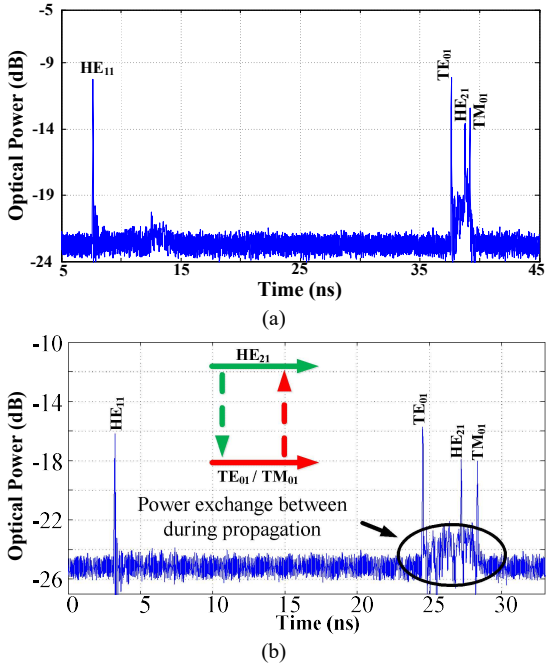

Fig. 2. ToF measurement results, (a) IPGIF (b) RCF

may be leakage between the excited HE_{11} and HE_{21} modes, as well as leakage from these excited modes to and from the parasitic TE_{01} and TM_{01} modes. In an OAM transmission system with separate mode detection, the mode demultiplexer is followed by two isolated and uncoordinated receivers: one for $OAM_0^{\pm}$ and one for $OAM_{\pm 1}$. There is no receiver for the TE_{01}/TM_{01} modes. The two isolated receivers will detect signals propagating along the direct path, but they will also receive leakage from other modes and the leakage from the same mode that goes back and forth between modes causing both interference (from the alternate information channel) and intersymbol interference (from the primary information channel).

The effective indices of TE_{01}/TM_{01} modes are close to HE_{21} in OAM fibers. Therefore, the interactions between [TE_{01}/TM_{01} and HE_{21}] tend to be stronger than both the crosstalk between [HE_{11} and HE_{21}] and the interactions between [HE_{11} and TE_{01}/TM_{01}]. Throughout this paper, we use $DMGD_{01}$ for the DMGD between HE_{11} and HE_{21} modes and $DMGD_{11}$ for the DMGD among vector modes HE_{21}, TE_{01} and TM_{01} that constitute OAM mode group one (OAM_1).

To study the impact of modal impairments, we examine RCF and IPGIF fibers, each supporting OAM modes of order zero and one. RCF is a step index fiber described in detail in [24], while IPGIF is a graded index fiber with an inverse parabolic index profile described in detail in [25]. Each fiber has distinct effective index separations among vector modes and

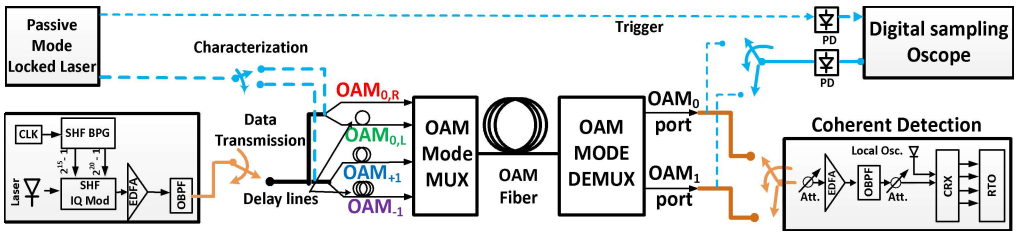

Fig. 3. OAM-MDM characterization and data transmission setup

distinct crosstalk levels and $DMGD_{01}$ and $DMGD_{11}$. The numerical aperture of the RCF and IPGIF fibers are 0.2959 and 0.1702, respectively. The loss of fibers using OTDR measurement without selective modal excitation at 1550 nm was measured as 3.8 dB/km and 2.8 dB/km for IPGIF and RCF, respectively. In next sections, we characterize the OAM-MDM link to observe and quantify the modal impairments in our OAM-MDM system.

III. OAM-MDM Link Characterization

In this section, we present ToF and IR measurements for an OAM-MDM system. These two experiments can give the same results in LP-MDM systems but in OAM-MDM systems using modes of order one, they will not give the same results. ToF measurement characterizes the interactions among all the supported vector modes during fiber propagation. This includes all the vector modes of HE_{11}, HE_{21}, TE_{01} and TM_{01}. IR characterizes the coupling among modes used as data channels in the OAM-MDM link, i.e HE_{11} and HE_{21}. In ToF experiments, we intentionally excite all vector modes (HE_{11}, HE_{21}, TE_{01} and TM_{01}) to observe the interactions among them during fiber propagation. In IR, we selectively excite and receive HE_{11} and HE_{21} modes using a mode mux and demux and observe the interactions between them. In IR measurements, however, power leakage leads to interactions among HE_{21} and TE_{01}/TM_{01} modes during fiber propagation and the powers that goes to TE_{01}, TM_{01} modes and come back to HE_{21} will be captured by this method.

A. Time of flight measurements

In ToF measurement, we generate a pulse train with 40 ps pulse width and 51.2 ns repetition rate and then using off-axis coupling to the fiber, *all* supported vector modes are excited simultaneously. The fiber output is detected by a high speed photodetector and recorded using a digital sampling oscilloscope (DSO). Results are presented in Fig. 2 for IPGIF and RCF. We adjusted the off-axis alignment until pulses with comparable power levels for all supported vector modes were observed. In both fibers, we observe four peaks corresponding to HE_{11}, TE_{01}, HE_{21} and TM_{01} modes. DMGD between vector modes are calculated from temporal separation of peaks in Fig. 2(a) and 2(b) and reported in Table I. Comparing the two fibers, RCF has larger $DMGD_{11}$ and smaller $DMGD_{01}$ than IPGIF. A prominent pedestal response is observed among TE_{01}, HE_{21} and TM_{01} in both fibers due to modal interactions; these modes continuously exchange power during propagation. The width of this pedestal is a little larger than $DMGD_{11}$. The impact of this pedestal on OAM-MDM performance will be investigated in later sections.

B. Channel impulse response

We measured channel impulse responses with the experimental setup in Fig. 3 with input and output connections in blue dashed lines. A passive mode locked fiber laser generates pulses with duration of ~10 ps with repetition rate of 50 ns. The demux output ports are captured by a DSO. We launched pulses on one channel at a time and recorded each demux output port. The technique of capturing one mode at a time in channel characterization was already discussed in [29]. Sixteen impulse responses measured for each fiber are shown in Fig. 4, arranged in a 4×4 channel matrix configuration; launched modes form columns, and received modes form rows. Some submatrices are magnified to better show the details.

The channel matrix is divided to four subsections for each fiber, labeled A through D. The 2×2 diagonal subsections (A and D) show interactions within each mode group, i.e., [OAM_0^+ with OAM_0^-] and [OAM_{+1} with OAM_{-1}]. The off-diagonal subsections (B and C) show interactions across mode groups. Since the channels inside each mode group are degenerate, there is strong coupling peaks in subsections A and D. For off-diagonal subsections, we observe two contributions to crosstalk: i) coupling at mux or demux appearing as sharp peaks, and ii) fiber coupling distributed over time that occurs throughout propagation.

In off-diagonal submatrices, B and C, the crosstalk from one mode group to the other is depicted. By comparing submatrices B and C for the two fibers, we observe more propagation crosstalk in IPGIF than RCF. We suspect the higher distributed mode coupling in IPGIF to be due to effects such as micro bending or fabrication imperfections.

We observe pulse broadening in subsection D for $OAM_{\pm1}$ modes, while the pulses remain sharp for OAM_0 in subsection A. To observe pulse broadening in greater details, we provide a zoom in for impulse responses of fibers for case of sending and receiving OAM_{+1} in Fig. 5. The width of measured pulses are 2.1 ns for IPGIF, 4.9 ns for 1.47 km RCF; width is calculated for values above the noise floor. These pulse widths are close to $DMGD_{11}$ measured by ToF, 1.7 ns for IPGIF and 3.8 ns for 1.47 km RCF. Using a full width 0.1 maximum definition, the IPGIF pulses are more broadened with a 2 ns width compared to 1.47 km RCF with a 0.6 ns width. Pulse broadening in a 450 m RCF fiber is also shown in Fig.5(b) with pulse widths of 0.3 ns and 0.4 ns using noise floor and full width 0.1 maximum pulse width definitions, respectively. The comparison of impulse responses of 1.47 km and 450 m RCF will be used in section V. to interpret the dependency of receiver performance to strength of modal interactions.

Table II
Measured crosstalk among OAM modes in OAM-MDM link for 1.47 km RCF and 1.1 km IPGIF

IPGIF	$HE_{11} \Rightarrow HE_{21}$	-7.7	$HE_{21} \Rightarrow HE_{11}$	-7.3
RCF	$HE_{11} \Rightarrow HE_{21}$	-10.7	$HE_{21} \Rightarrow HE_{11}$	-10.6

C. *Crosstalk measurements*

To complement IR measurements, we also measure total crosstalk among mode groups. Crosstalk measurement is done with the same signal source used for data transmission: a 16 Gbaud QPSK signal on two polarizations (setup described in detail in the next section).

We used a power meter to measure the received power at demultiplexer output port when transmitting two polarizations of the corresponding or the other mode group. The crosstalk is

$$\text{Crosstalk on } OAM_i = 10\log\left(P_{|i-1|}/P_i\right) \qquad i \in \{0,1\} \qquad (5)$$

Results are reported in Table II. Crosstalk is lower in RCF, consistent with IR matrices. We also measured the crosstalk from MUX and DEMUX stages using a 1m RCF fiber, where the propagation crosstalk in the fiber is negligible. This crosstalk was around -20 dB.

D. *Interpretation of system characterizations*

In ToF, we excited all vector modes and observed a pedestal response among HE_{21} and TE_{01}/TM_{01} due to continuous interactions among these vector modes during propagation. In IR measurements, we launched one targeted mode at a time, i.e., $OAM_0^{\pm}$ or $OAM_{\pm1}$, and captured each demux output. In IR measurements the pulse in $OAM_{\pm1}$ modes is broadened with a width similar to the ToF pedestal width. We conclude pulse broadening is due to power exchange within mode group one: HE_{21} leaking to/from parasitic modes TE_{01} and TM_{01}. This modal mixing can occur in fiber or mode (de)mux. Note that, unlike the ToF setup, in IR measurement, we do *not* excite TE_{01} and TM_{01} modes. Their effect is inferred from the pulse broadening in HE_{21} mode matching the pedestal width in ToF measurements. The parasitic modes of TE_{01}/ TM_{01} may be incidentally excited during mux and/or demux; they may arise during coupling in the fiber propagation. The reason that the pedestal around HE_{21} has a higher power level in ToF compared to IR is that, in ToF, TE_{01} and TM_{01} are intentionally excited at the input of fiber with the power comparable to HE_{21}. This observation means that although TE_{01}/TM_{01} modes are not used as data carrying channels, they can affect receiver performance by pulse broadening in $OAM_{\pm1}$ modes resulting in intersymbol interference (ISI) among consecutive data symbols transmitted in $OAM_{\pm1}$ channels. Such phenomena can affect the memory depth requirement for receiver equalizers and will be discussed in the next section via data transmission results.

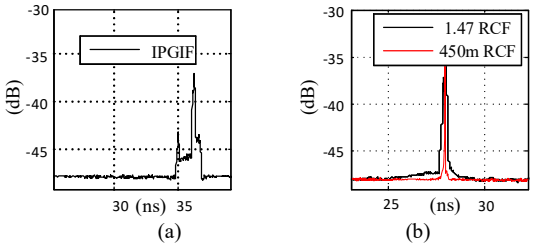

Fig. 5. Enlarged channel impulse response for case of sending and receiving OAM_{+1} in (a) IPGIF (b) 1.47 km and 450 m RCF

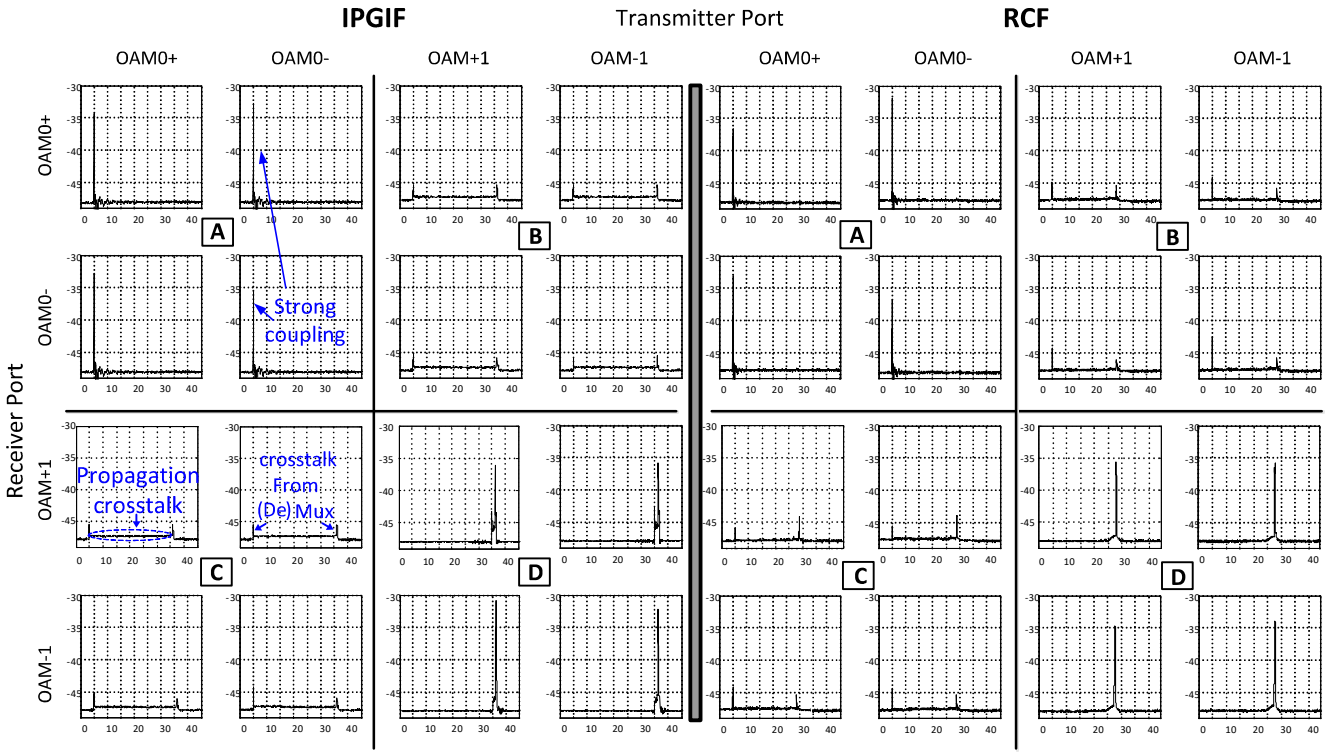

Fig. 4. Channel impulse response for OAM-MDM link using 1.2 km IPGIF (left) and 1.47 km RCF (right) with scales of (dB) and (nsec) on x and y axes of sub figures.

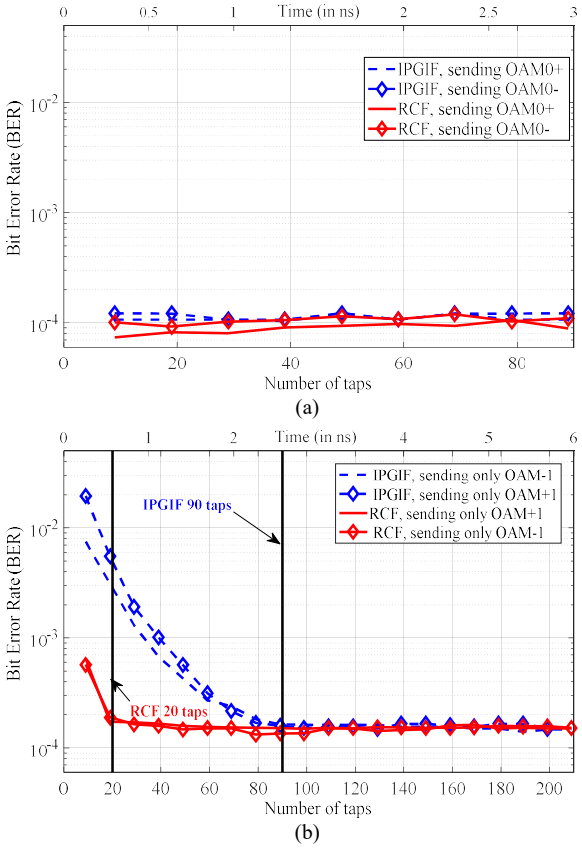

Fig. 6. BER at OSNR = 16 dB vs. number of taps, (a) sending only $OAM_0^{\pm}$, (b) sending only $OAM_{\pm1}$; IPGIF is 1.2 km, RCF is 1.47 km.

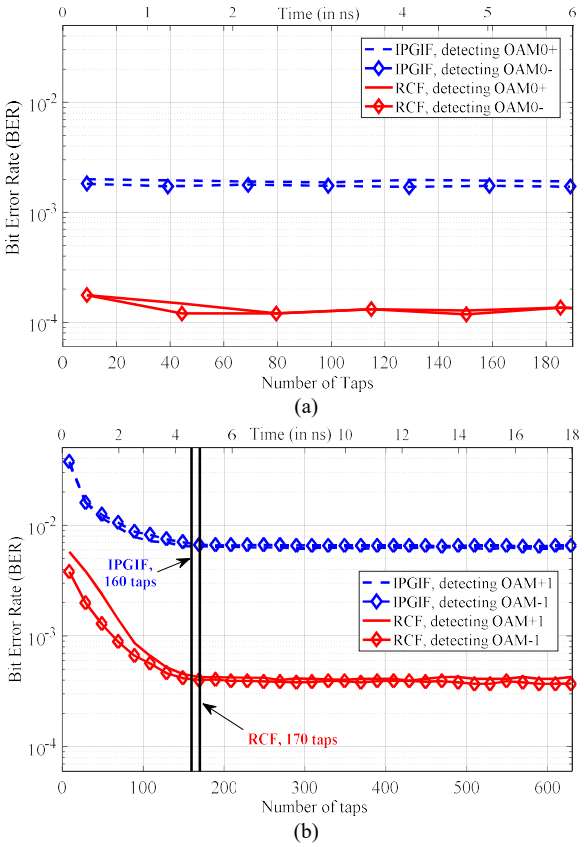

Fig. 7. BER at OSNR = 25 dB vs. number of taps, sending all modes and (a) detecting $OAM_0^{\pm}$, (b) detecting $OAM_{\pm1}$; IPGIF is 1.2 km, RCF is 1.47 km.

IV. Data Transmission in OAM-MDM Link

In this section, we discuss data transmission results for four channels ($OAM_0^{\pm}$ and $OAM_{\pm1}$) over RCF and IPGIF fibers. In section A, we briefly describe the data transmission setup. In Section B, we evaluate the receiver BER and discuss the impact of modal impairments on system performance and equalizer memory depth for RCF and IPGIF fiber. In section C we examine RCF fiber of different lengths.

A. Data transmission setup

Fig. 3 shows the data transmission setup; input switches are set for data and output switches are set for coherent detection. A single polarization non-return-to-zero (NRZ) QPSK signal at baudrate of 16 Gbaud is generated via a bit pattern generator (BPG) with two pseudo random binary sequences (PRBS) of length 2^{15}-1 and 2^{20}-1 and an MZM IQ modulator. The transmitter laser has a linewidth of 100 kHz and is set to 1550 nm with output power of 16 dBm; the generated QPSK signal is amplified and then sent to the OAM-MDM link.

By using delay lines, four decorrelated replicas of the signal are generated. These four decorrelated signals are input to a mode multiplexer where two of them are mapped on $OAM_{\pm1}$ modes and combined with the two on $OAM_0^{\pm}$ mode. They are then coupled to the OAM fiber. After propagation over OAM fiber, the two mode groups are separated in the polarization diverse mode demultiplexer and sent to data recovery setup separately. A single coherent receiver (CRX) with bandwidth of 22 GHz and a local oscillator with linewidth of 10 kHz and output power of 13 dBm are used to coherently detect the incoming signal, either two polarizations of OAM_0 or $OAM_{\pm1}$. The output electrical signals from the coherent receiver are captured by a Keysight real-time oscilloscope (RTO) with 33 GHz analog bandwidth capturing data at 80 Gsample/s; afterwards the DSP is applied offline. The offline DSP is the same as that used in dual-polarization, single-mode coherent detection, including blocks of resampling, 2×2 equalization among two polarizations of each mode, frequency offset estimation and carrier phase recovery.

B. BER and required memory depth for RCF and IPGIF

We ran data transmission, evaluated BER and determined required memory depth in two scenarios - sending only one mode group (two channels) or sending all channels. Transmitting only one mode excludes the impact of crosstalk across mode groups. Sections A and D of channel matrices apply to sending only $OAM_0^{\pm}$ and $OAM_{\pm1}$ respectively. BER versus number of taps per equalizer are presented in Fig. 6 (a) and (b) for $OAM_0^{\pm}$ and $OAM_{\pm1}$, respectively.

When sending only $OAM_0^{\pm}$, we do not observe any meaningful BER dependency on equalizer memory depth; even small equalizer lengths reach the minimum of BER for both fibers. The minimum achievable BER is the same for both fibers. When sending only $OAM_{\pm1}$, we reach the minimum of BER with 20 and 90 half-symbol-spaced taps for RCF and

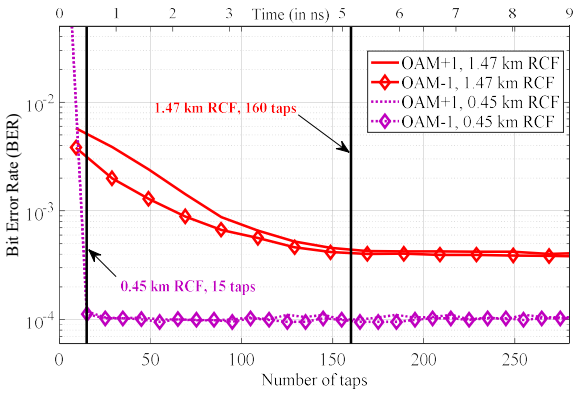

Fig. 8. BER vs number of taps for $OAM_{\pm1}$ channels, RCF fibers of 1.47 km at OSNR=25 dB and 450 m at OSNR=16 dB

IPGIF, respectively, corresponding to 0.625 ns and 2.8 ns. The required equalizer memory depth is due to pulse broadening in $OAM_{\pm1}$ channels. Increasing the number of equalizer taps compensates for ISI due to pulse broadening.

Next, we report in Fig. 7, the BER versus number of taps when sending both mode groups (all 4 data channels). Fig. 6(a), (b) show the BER at the receiver for the zero and one order modes, respectively. Comparing Fig. 5 (one mode at a time) and Fig. 6 (all modes), achievable BER is lower and there is an OSNR penalty to reach that BER. Note measurements in Fig. 6 and Fig. 7 are evaluated at OSNRs of 16 dB and 25 dB, respectively. When sending all channels, regardless of memory depth used, RCF fiber always outperforms IPGIF on all data channels due to lower crosstalk.

For $OAM_0^{\pm}$, Fig. 7(a), we again observe no BER dependency on equalizer memory depth. For $OAM_{\pm1}$, Fig. 7(b), beside the OSNR penalty, we observe more required taps for both fibers to reach the minimum of BER compared to the crosstalk-free case of Fig. 6(b). We reach the minimum of BER with 160 taps (5 ns) for IPGIF and 170 taps (5.3 ns) for RCF. The reason for increased number of taps, compared to the case of sending only $OAM_{\pm1}$, is the crosstalk from $OAM_0^{\pm}$ channels as discussed in the next section.

C. BER and required memory depth for two lengths of RCF

To further investigate the impact of crosstalk from $OAM_0^{\pm}$ on equalizer memory depth in $OAM_{\pm1}$ channels, we examine a 0.45 km RCF fiber with crosstalk of -15.5 dB between $OAM_0^{\pm}$ and $OAM_{\pm1}$. $DMGD_{01}$ and $DMGD_{11}$ can be inferred from the 1.47 km fiber measurement using the ratio of fiber lengths ($0.45/1.47 \approx 0.3$). $DMGD_{11}$ is about1.26 ns for the shorter fiber. In Fig. 8 we compare BER performance for $OAM_{\pm1}$ channels for these two RCF lengths. The required memory depth to reach minimum BER for 0.45 km fiber is around 15 taps or ~0.47 ns, which is smaller than its $DMGD_{11}$. The required memory depth for 1.47 km fiber at minimum BER is around 160 or 5 ns, which is larger than its $DMGD_{11}$. In next section, we discuss the relationship between memory depth requirement and modal interactions observed in section III.

V. Discussion on Receiver Performance and Complexity

We summarize the parameters related to receiver complexity for $OAM_{\pm1}$ channels that were estimated in experiments in Table IV. In the first column, we have the crosstalk from $OAM_0^{\pm}$ on $OAM_{\pm1}$. In the other columns are time constants measured first in characterizing the fibers and then via BER evaluation (equalizer memory depth).

Consider RCF and IPGIF at lengths above a kilometer. The pulse broadening (Fig. 4) when measured as all points above the noise floor is reasonably close to $DMGD_{11}$ measured in ToF (Fig. 2). $DMGD_{11}$ measures time between peaks, but not the edges of the interactions on either side of these peaks, hence it is natural that $DMGD_{11}$ is smaller than the pulse broadening. This time constant is closely related to the equalizer memory depth when sending all modes (darker shading on these values).

Pulse broadening at full width 0.1 maximum is a close match to memory depth of equalizers when sending only $OAM_{\pm1}$, i.e., with no crosstalk present (lighter shading on these values). We probed the level of broadening having significant impact on DSP complexity, and settled on the 0.1 maximum value.

The interactions among TE_{01}/TM_{01} and HE_{21} are the primary source of intersymbol interference, as data moves between the three vector modes. These strong modal interactions lead the full width 0.1 maximum pulse broadening of IPGIF to be nearly equal to the noise floor broadening measurement; the broadened pulse is nearly rectangular. With lower interactions in RCF, the broadened pulse rolls off more slowly.

When sending only $OAM_{\pm1}$, crosstalk is absent and ISI is the only impairment to overcome. Hence, the equalizer memory depth is determined by a time constant nuanced with the level of interaction within the mode group, i.e., the full width 0.1 maximum pulse broadening. Note that equalizer memory depth will always be larger than the relevant time constants to compensate the other impairments as well (e.g., imperfect sampling, limited RF bandwidth, limited sample resolution, etc.) [30], [31].

When sending all channels and detecting $OAM_{\pm1}$, crosstalk

Table IV. Summary of parameters in characterization and data transmission related to memory depth of equalizers

Fiber	Characterization measurements				Data transmission	
	crosstalk	ToF	impulse response		equalizer memory depth	
	HE_{11} on HE_{21}	$DMGD_{11}$	pulse broadening: noise floor	pulse broadening: 10dB	sending only $OAM_{\pm1}$	sending all modes
RCF 1.47 km	-10.5 dB	3.8 ns	4.9 ns	0.6 ns	0.62 ns	5.3 ns
IPGIF 1.10 km	-7 dB	1.7 ns	2.1 ns	2.0 ns	2.8 ns	5 ns
RCF 0.45 km	-15.5 dB	1.26 ns	0.4 ns	0.3 ns	–	0.5 ns

from $OAM_0^{\pm}$ is present as well as ISI. The memory depth is increased as the equalizer uses more taps to gather energy from the desired signal to overcome crosstalk. The relevant time constant is now the $DMGD_{11}$. The equalizer scavenges all available traces of the desired signal in the isolated, single port to which it has access. By exceeding the $DMGD_{11}$ (which measures time between peaks, but not the edges of the interactions on either side of these peaks), our equalizers collect signal energy in HE_{21} that goes to TE_{01}/TM_{01} and HE_{11} and comes back to HE_{21} in the enlarged time span. Furthermore, by using a higher memory depth, the errors due to pulse broadening from a larger number of adjacent symbols will be corrected. Without full MIMO, i.e., without access to data leaked to the unobserved port, the receiver has very limited improvement for memory depth significantly beyond $DMGD_{11}$, as seen in the BER floor.

Finally, we compare the two RCF fibers of length 0.45 km and 1.47km. The $DMGD_{11}$ scales linearly with fiber length, but equalizer memory depth is more than 10 times larger for the longer fiber. The crosstalk is more than 3 times larger in the longer fiber. This reinforces our argument that larger crosstalk leads to memory depth greater than $DMGD_{11}$. In the shorter fiber where the BER penalty due to crosstalk is negligible, the memory depth is much smaller (.5 ns) than $DMGD_{11}$, (1.26 ns). Tap number reduction exceeding the ratio of RCF lengths can be attributed to differences in pulse broadening. In Fig. 5(b), where pulse broadening in 1.47 km and 450m RCF is depicted, tails of the impulse response at 450 m are much less extensive than those in the longer fiber; at 450 m the pulse broadening gives very consistent figures of merit (full width 0.1 maximum pulse width or noise floor pulse width).

Time domain equalization was used to facilitate interpretation of results, in particular the relevance of time constants observed in our ToF and impulse response characterizations. A practical system would use frequency domain equalization for memory depth greater than 16 taps [32].

VI. Conclusion

We observed different memory depth requirements in reception of data carried by OAM modes of order zero and one. We investigated the source of this difference via channel characterization and data transmission. Unlike LP-MDM, TE_{01}/ TM_{01} modes are not data carrying for OAM-MDM. These modes are nonetheless incidentally excited, and therefore become parasitic modes in the fiber, interacting with data carrying modes. Their interaction with HE_{21} can result in pulse broadening and ISI for data transmitted in $OAM_{\pm1}$ channels. Results shows that memory depth of equalizers in $OAM_{\pm1}$ channels is directly related to this phenomenon, as well as channel crosstalk. For OAM-MDM systems targeting a low complexity receiver, the interactions between data carrying HE_{11} and HE_{21} modes and non-data carrying TE_{01}/ TM_{01} should be minimized in fiber design. If this is not possible, higher order modes may be more appropriate as their interaction with parasitic modes would be much reduced.

VII. References

[1] René-Jean Essiambre, G. Kramer, P. J. Winzer, G. J. Foschini, and B. Goebel, "Capacity limits of optical fiber networks," *J. Lightw. Tech.*, vol. 28, no. 4, pp. 662–701, Feb. 2010.

[2] P. J. Winzer, "Energy-efficient optical transport capacity scaling through spatial multiplexing," *IEEE Photon. Technol. Lett.*, vol. 23, no. 13, pp. 851–853, Jul. 2011.

[3] Ezra Ip, G. Milione, N. Cvijetics, M.-J. Li, J. Downie, "High capacity Optical Transmission Systems using Spatial Division multiplexing," *Photonics in Switching*, 2015: Invited papers.

[4] Roland Ryf, S. Randel, A. H. Gnauck, C. Bolle, A. Sierra, S. Mumtaz, M. Esmaeelpour, E. C. Burrows, R-J. Essiambre, P. J. Winzer, D. Peckham, A. McCurdy, and R. Lingle, "Mode-division multiplexing over 96 km of few-mode fiber using coherent 6×6 MIMO processing," *J. Lightw. Technol.*, vol. 30, no. 4, pp. 521–531, Feb. 2012.

[5] Nenad Bozinovic, Y. Yue, Y. Ren, M. Tur, P. Kristensen, H. Huang, A. E. Willner, S. Ramachandran, "Terabit-Scale Orbital Angular Momentum Mode Division Multiplexing in Fibers," *Science*, vol. 340, pp. 1545-1548, Jun. 2013.

[6] Long Zhu, A. Wang, S. Chen, J. Liu, C. Du, Q. Mo and J. Wang, "Experimental Demonstration of Orbital Angular Momentum (OAM) Modes Transmission in a 2.6 km Conventional Graded-Index Multimode Fiber Assisted by High Efficient Mode-Group Excitation," *in Proc. Opt. Fiber Commun. Conf.* (OFC) 2016, W2A.32.

[7] Joel Carpenter, B. C. Thomsen, and T. D. Wilkinson, "Degenerate Mode-Group Division Multiplexing," *J. Lightw. Technol.*, vol. 30, no. 24, pp. 3946-3952, Dec. 2012.

[8] Giovanni Milione, H. Huang, M. P. J. Lavery, T. A. Nguyen, G. Xie, Y. Cao, M. Willner, M. Tur, S. Dolinar, R. R. Alfano, M. J. Padgett, and A. E. Willner, "Orbital-Angular-Momentum Mode (De)Multiplexer: A Single Optical Element for MIMO-based and non-MIMObased Multimode Fiber Systems," *in Proc. Opt. Fiber Commun. Conf.* (OFC) 2014, M3K.6.

[9] Jun Liu, S. Li, Y. Ding, A. Wang, L. Zhu, S. Li, S. Zheng, S. Chen, S. Yu, X. Cai, and J. Wang, "Demonstration of Orbital Angular Momentum (OAM) Modes Emission from a Silicon Photonic Integrated Device for 20 Gbit/s QPSK Carrying Data Transmission in Few-Mode Fiber," *in Proc. Conf. Laser and Electro-Optics* (CLEO) 2016, JTh2A.129.

[10] Feng Feng, Xianqing Jin, Dominic O'Brien, Frank. P. Payne, Timothy D. Wilkinson, "Mode-Group Multiplexed Transmission using OAM modes over 1 km Ring-Core Fiber without MIMO Processing," *in Proc. Opt. Fiber Commun. Conf.* (OFC) 2017, Th2A.43.

[11] Nicolas K. Fontaine, R. Ryf, H. Chen, A. V. Benitez, B. Guan, R. Scott, B. Ercan, S. J. B. Yoo, L. E. Grüner-Nielsen, Y. Sun, R. Lingle, E. Antonio-Lopez, and R. Amezcua-Correa, "30×30 MIMO transmission over 15 spatial modes," in *Proc. Opt. Fiber Commun. Conf.* (OFC) 2015, Postdeadline Paper, Th5C.1.

[12] Roland Ryf, H. Chen, N. K. Fontaine, A. M. Velazquez-Benitez, José Antonio-Lopez, C. Jin, B. Huang, M. Bigot-Astruc, D. Molin, F. Achten, P. Sillard, R. Amezcua-Correa, "10-Mode mode-multiplexed transmission over 125-km single-span multimode fiber," in *Proc. Eur. Conf. Opt. Commun.* (ECOC), 2015.

[13] Philippe Genevaux, C. Simonneau, G. Labroille, B. Denolle, O. Pinel, P. Jian, J.-F. Morizur, G. Charlet, "6-mode Spatial Multiplexer with Low Loss and High Selectivity for Transmission over Few Mode Fiber," *in Proc. Opt. Fiber Commun. Conf.* (OFC) 2015, W1A.5.

[14] Massimiliano Salsi, Clemens Koebele, Gabriel Charlet, Sébastien Bigo, "Mode Division Multiplexed Transmission with a weaklycoupled Few-Mode Fiber," in Proc. Opt. Fiber Commun. Conf. (OFC) 2012, OTu2C.5

[15] Ezra Ip, G. Milione, Ming-Jun Li, Neda Cvijetic, Konstantinos Kanonakis, Jeffery Stone, Gaozhu Peng, Xesús Prieto, Carlos Montero, Vicente Moreno, and Jesús Liñares, "SDM transmission of real-time 10GbE traffic using commercial SFP + transceivers over 0.5km elliptical-core few-mode fiber," *Opt. Exp.,* vol. 23, no. 13, pp. 17120-17126, Jun 2015.

[16] Ezra Ip, N. Cvijetic, G. Milione, K. Kanonakis, T. Wang, M.-J. Li, J. Stone, G. Peng, "MIMO Equalization Analysis for SDM Transmission Over 2km Elliptical-Core Few-Mode Fiber for Datacenter Applications," *Proceedings of APCC* 2015.

[17] L. Wang, R. M. Nejad, A. Corsi, J. Lin, Y. Messaddeq, L. A. Rusch, and S. LaRochelle, "MIMO-Free Transmission over Six Vector Modes in a Polarization Maintaining Elliptical Ring Core Fiber," *in Proc. Opt. Fiber Commun. Conf.* (OFC) 2017, Tu2J.2, 2017.

[18] Nenad Bozinovic, P. Kristensen, and S. Ramachandran, "Long-range fiber-transmission of photons with orbital angular momentum", *in Proc. Conf. Laser Opt. elec.* (*CLEO*) 2011, CTuB1.

[19] Patrick Gregg, P Kristensen, and S. Ramachandran, "13.4km OAM state propagation by recirculating fiber loop," Opt. Exp., vol. 24, no. 17, pp. 18938-18947, Aug 2016.

[20] Reza Mirzaei Nejad, K. Allahverdyan, P. Vaity, S. Amiralizadeh, C. Brunet, Y. Messaddeq, S. LaRochelle, and L. A. Rusch, "Mode Division Multiplexing Using Orbital Angular Momentum Modes Over 1.4-km Ring Core Fiber," *J. Lightwave Technol.*, vol. 34, no. 18, pp. 4252-4258, Sept. 2016.

[21] Kasper Ingerslev et al., "12 Mode, MIMO-Free OAM Transmission," *in Proc. Opt. Fiber Commun. Conf. (OFC) 2017*, M2D.1.

[22] K.-P. Ho and J. M. Kahn, "Linear propagation effects in mode-division multiplexing systems," *J. Lightw. Technol.*, vol. 32, no. 4, pp. 614–628, Feb. 2014.

[23] Xianqing Jin, A. Gomez, K. Shi, B. C. Thomsen, F. Feng, G. S. D. Gordon, T. D. Wilkinson, Y. Jung, Q. Kang, P. Barua, J. Sahu, S. Alam, D. J. Richardson, D. C. O'Brien, and F. P. Payne , "Mode Coupling Effects in Ring-Core Fibers for Space-Division Multiplexing Systems," *J. Lightw. Technol*., vol. 34, no. 14, pp. 3365-3372, Jul. 2016.

[24] Charles Brunet, B. Ung, L Wang, Y. Messaddeq, S. LaRochelle, and L. A. Rusch, "Design of a family of ring-core fibers for OAM transmission studies," *Opt. Exp.*, vol. 23, no. 8, pp.10553-10563, 2015.

[25] Bora Ung, P. Vaity, L. Wang, Y. Messaddeq, L. A. Rusch, and S. LaRochelle, "Few-mode fiber with inverse-parabolic graded-index profile for transmission of OAM-carrying modes," *Opt. Exp.*, vol. 22, no. 15, pp. 18044–18055, Jul. 2014.

[26] Reza Mirzaei Nejad, K. Allahverdyan, C. Brunet, S. LaRochelle and L. A. Rusch, "Experimental Study of Receiver Complexity in OAM-MDM Transmission Systems," *2016 IEEE Photonics Conference* (IPC), Waikoloa, 2016, TuB2.4.

[27] Reza Mirzaei Nejad, L. Wang, J. Lin, S. LaRochelle, L. A. Rusch, "Parasitic Effect of TE and TM modes in OAM-MDM Transmission Systems," *in Proc. Conf. Laser and Electro-Optics* (CLEO), San Jose, CA, 2017, SW4I.2.

[28] P. Z. Dashti, F. Alhassen, and H. P. Lee, "Observation of orbital angular momentum transfer between acoustic and optical vortices in optical fiber,"Phys. Rev. Lett., vol. 96, p. 043604, Feb. 2006.

[29] Kai Shi, A. Gomez, X. Q. Jin, Y. Jung, C. Quintana, D. C. O'Brien, F. P. Payne, P. Barua, J. Sahu, Q. Kang, S.-U. Alam, D. J. Richardson, and B. C. Thomsen, "Simplified impulse response characterization for mode division multiplexed systems," *in Proc. Opt. Fiber Commun. Conf.* (OFC) 2016, W4F.3.

[30] Seb J. Savory "Digital Coherent Optical Receivers: Algorithms and Subsystems," *IEEE J. Sel. Topics Quantum Electron*., vol. 16, no. 5, pp. 1164-1179, Sep. 2010.

[31] Kazuro Kikuchi, "Clock recovering characteristics of adaptive finite-impulse-response filters in digital coherent optical receivers," *Opt. Exp.*, vol. 19, no. 6, pp. 561114- 561119, Mar 2011.

[32] Randel, P. J. Winzer, M. Montoliu and R. Ryf, "Complexity analysis of adaptive frequency-domain equalization for MIMO-SDM transmission," in *Proc. Eur. Conf. Opt. Commun.* , (ECOC) 2013.